PCCP
Physical Chemistry Chemical Physics

Accepted Manuscript

This article can be cited before page numbers have been issued, to do this please use: A. Veit Berg, A. Forster, T. Hansson, A. J. S. Jernstedt, E. Salminen and E. Schröder, *Phys. Chem. Chem. Phys.*, 2026, DOI: 10.1039/D6CP01070A.

View Article Online
DOI: 10.1039/D6CP01070A

First-principle study of the influence of hydroxyapatite on magnesium surfaces

Anthony Veit Berg, Ablai Forster, Tim Hansson, Alex J. Jernstedt, Emmy Salminen, and Elsebeth Schröder*
Department of Microtechnology and Nanoscience, MC2,
Chalmers University of Technology, SE-41296 Göteborg, Sweden
(Dated: June 9, 2026)

Hydroxyapatite (HA) on a magnesium (Mg) surface is studied using density functional theory, to help understand the effect of HA coating and alloying in the surfaces of Mg-based biodegradable implants. We determine the adsorption energies and structural changes of a single layer of HA on pure Mg(0001) and on sparsely calcium (Ca) or zinc (Zn) doped Mg(0001) and find that both Zn and Ca doping improves the adsorption, except in a few positions of HA relative to the dopant position. All adsorption configurations, whether with pure or doped Mg surfaces, show deformation of the surface and HA layer. For Ca doping, we found that for a certain adsorption configuration, the dopant Ca atom moves out of the Mg surface and into the HA layer, leaving behind a Mg vacancy in the top layer of the Mg surface. Plots of electron density changes show that electrons accumulate around the Ca dopant and the neighboring Mg atoms, while in Zn doping this is less pronounced. Overall, our results demonstrate that the dopant choice and relative position of HA influence the interaction between HA and Mg-surfaces, and affect both adsorption energies and atomic and electronic structures.

Keywords: density functional theory, magnesium, hydroxyapatite, vdW-DF-cx

I. INTRODUCTION

Orthopedic implants are used to stabilize fractures and replace damaged tissue. In practice, metals like titanium, cobalt chromium alloys and stainless steel are often used because they tolerate high loads and wear [1]. Magnesium (Mg) has also gained interest for orthopedic implants due to its biocompatibility, mechanical compatibility with bone and since it naturally degrades within the human body [2]. Many alloys currently used for implants are much stiffer than bone, causing the implant to absorb mechanical load. As a result, stress shielding slows down the healing process [3]. The stiffness of Mg, on the other hand, resembles that of natural bone better [4].

Mg corrodes easily due to its low electrochemical potential. This leads to a release of Mg ions, which are naturally present in the body and are thought to support bone healing [5, 6]. Titanium implant materials, such as Ti-6Al-4V, may pose safety concerns with long-term release of vanadium or aluminum since these elements could be a probable cause for osteomalacia, peripheral neuropathy and Alzheimer's disease [7]. For Mg the main concern is the fast corrosion rate of pure Mg, which may lead to H_2 and other gas cavities that could damage nearby tissue, and in severe cases cause necrosis [2, 8], although in some studies the gas is found to mostly modify the local environment rather than being harmful per se [9]. As degradation progresses, the implant may fragment under physiological compressive loads. This damage can propagate as penetrating cracks, resulting in a loss of mechanical integrity [10].

Given the challenges associated with Mg degradation, many Mg-based alloys and coatings have emerged as promising approaches to help implants last longer and support bone regeneration. For example, Mg alloyed with small amounts of Zn and Ca shows good biocompatibility [11], and after immersion in simulated body fluid such surfaces show sign of forming magnesium hydroxide ($Mg(OH)_2$) and hydroxyapatite (HA) [12, 13]. Further, HA has a tendency to adhere to Mg-based substrates, building up full coverage layer by layer [14], indicating its potential to serve as a protective layer that mitigates the degradation of an implant [14–19].

In this study, density functional theory (DFT) calculations are used to examine the stability of HA coatings on Mg-based surfaces, including the effects of sparse zinc (Zn) or calcium (Ca) alloying of the Mg surface. We determine adsorption energies and structures, and study the changes in electron distribution that arise from the adsorption. Our results provide insight into factors influencing the adsorption and stability of HA on these surfaces.

The text is organized as follows: Section II describes the materials while Section III outlines the methods. Section IV presents and discusses the results, and Section V contains our conclusions and a summary.

II. MATERIALS

The choice of implant material depends on many factors. It is often desirable for implant materials to have a stiffness (Young's modulus) that is comparable to bone to avoid stress shielding. The elastic modulus in the bone, depending on the site and bone type, is roughly 4-30 GPa [20]. Mg has a Young's modulus of approximately 44 GPa and resembles the stiffness of natural bone better than other commonly used metals [4]. By comparison, stainless steel and Co-Cr have a Young's moduli around 200-240 GPa and the widely used Ti-6Al-4V near 110

* Corresponding author; schroder@chalmers.se (E. Schröder)

View Article Online
DOI: 10.1039/D6CP01070A 2

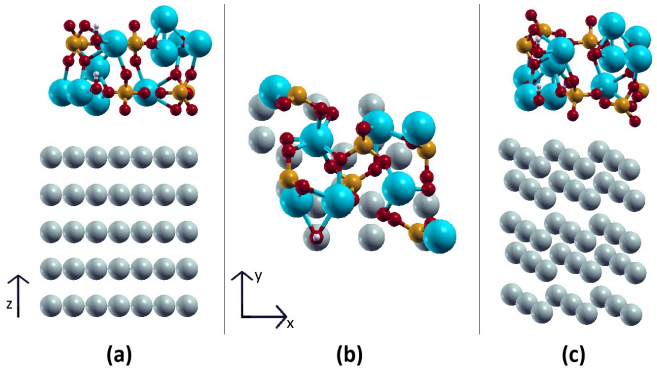

FIG. 1. Hydroxyapatite (HA) on the Mg(0001) surface, shown from three perspectives to illustrate the structural arrangement and relative positioning. (a) Side view (x-z plane). (b) Top view (x-y plane). (c) Angled view. Color coding of atoms: magnesium - grey, oxygen - red, phosphorus - orange, calcium - blue, hydrogen - white. All structures and electron densities visualized with XCrySDen.

GPa [21]. If the implant cannot stay permanently in the body (e.g., growing bone in children), a further drawback of stainless steel and Ti-6Al-4V is that a second surgery may be needed for removal [22], while Mg degrades and the challenge there is to have it degrade at a pace corresponding to the healing of the bone. Alloying and coating are methods to inhibit the corrosion.

For modelling coating we here use a layer of HA on top of the Mg(0001) surface, either on pristine Mg(0001) or with sparse doping of Zn or Ca. Figure 1 provides an overview of the combined structure of HA on Mg(0001) as seen from the side, the top and a tilted side view, with the cartesian coordinate system used later indicated in (a) and (b). The figure shows an isolated HA layer rigidly put on top of pure Mg(0001), unaffected by the presence of the HA layer and before any deformations of Mg(0001) or HA have been taken into account. All structures and electron densities are visualized with XCrySDen [23].

A. Mg(0001) with alloys

The crystalline structure of Mg bulk at ambient conditions is the hexagonal close-packed (hcp) structure. With the methods used here, the lattice parameters are found [24] to be $a = 3.192$ Å and $c = 5.186$ Å. We study the basal plane Mg(0001) which is the most stable direction and which is commonly used for surface calculations in DFT studies due to its simple, unreconstructed structure [25–32], while other low-index directions such as the prismatic $(10\bar{1}0)$ and pyramidal $(10\bar{1}1)$ have higher reactivity [33, 34]. For its simplicity and compatible surface unit cell size relative to HA, Mg(0001) is chosen here as a model structure to investigate interactions with HA.

Surface doping of Mg(0001) with Zn and Ca is of particular interest due to their compatibility with Mg and their natural occurrence in the human body. Zn is an essential mineral which has vital functions in the body, some being catalytic activity of enzymes, protein- and DNA synthesis [35]. The crystalline structure of Zn, like Mg, is hcp, making Zn compatible with the structure of Mg(0001) [36]. Studies have shown that corrosion rates of Mg decrease with Zn alloying and that the rates depend on the Zn content [37, 38].

Ca, on the other hand, is the most abundant mineral in the body [39]. It is an essential mineral (like Zn) and a main component of HA found in bones and teeth. The corrosion behavior can improve with Mg-Ca alloys, and also for Ca, the corrosion rate depends on the Ca content [40]. Ref. [11] reported that an Mg-Ca alloy implant immersed in Hank's balanced salt solution showed excellent biocompatibility, with formation of HA on the surface, while Ref. [41] reported HA formation on the surface of a Mg-Ca alloy with 1 weight percent (wt%) of Ca during both in vitro and in vivo corrosion.

B. Hydroxyapatite

HA is a calcium phosphate that is one of the main components of human bone [42]. It is widely recognized for its osteoconductivity and biocompability and shows great potential to be used in areas like bone tissue engineering [43, 44]. Due to its brittleness and low fatigue resistance, HA is not suitable as a load-bearing implant and it is primarily used in non-load-bearing applications [45–49]. However, applying HA as a surface coating on metals can affect the corrosion behavior and the properties of the material, which could be useful in implant applications [18, 50, 51].

III. METHODS

A. Density functional theory modelling of Mg(0001)

Our results are based on DFT calculations with the van der Waals-inclusive functional vdW-DF-cx [52–55], using the plane wave code `pw.x` for the DFT calculations and `pp.x` for postprocessing, both codes from the Quantum ESPRESSO suite [56–58]. We use PAW-based pseudopotentials from PSLibrary [59, 60] to describe the atoms, except for Mg, which is described by a PAW pseudopotential that one of us created and thoroughly tested in Ref. [24].

The Mg(0001) surface is modeled by slabs with periodic boundary conditions, in surface unit cells that consist of 3×3 hcp bulk unit cells laterally and 5 layers of Mg as thickness of the slab. This lateral size is chosen as it approximately fits with one unit cell of HA. All surface calculations have vacuum added on top, in order to avoid interactions with repeated slabs along the z-direction. This leads to a total cell size of 36 Å in height, leaving around 16 Å of vacuum above the slab when HA

View Article Online
DOI: 10.1039/D6CP01070A

is added on Mg(0001). The bottom three Mg layers are kept fixed in the atomic positions obtained from a calculation with a fully relaxed slab of 23 layers [24, 61, 62], while all other atoms are allowed to move according to the Hellmann-Feynman forces (except when stated).

B. Convergence tests and computational parameters

Aiming for a calculational accuracy of at least 10 meV per supercell we carried out convergence studies of the number of Monkhorst-Pack [63] k-points needed in the supercell with HA included, as well as the plane wave energy cutoff for the kinetic energy, $E_{\rm cut}$ and electron density $E^{\rho}_{\rm cut}$. The k-point convergence test was conducted using $n_k \times n_k \times 1$ grids with n_k = 2, 4, 6, 8, 10, and 12. For each mesh, a standard relaxed HA-on-Mg(0001) structure was calculated. Then, the HA layer was uniformly moved 0.1 Å away from Mg(0001) and a new calculation with fixed atom positions was performed on the structure. From the difference in total energy between these two configurations we found that the best balance between calculation accuracy and computational cost was obtained with the $6 \times 6 \times 1$ k-point mesh.

In a similar series of test calculations for energy cutoffs of the plane-wave basis, $E_{\rm cut}$, and electron density, $E^{\rho}_{\rm cut}$, we tested values 40/320, 50/400, 60/480 and 70/560 Ry, using the $6 \times 6 \times 1$ k-point mesh, and found the optimal values $E_{\rm cut}$ = 50 Ry and $E^{\rho}_{\rm cut}$ = 400 Ry. These are the values we use throughout this study.

To report directional changes in atomic positions and changes in atom-atom distances we introduce a cartesian coordinate system as indicated in Figure 1, with x- and y-directions in the Mg surface (0001) plane and z in the [0001] direction.

C. Adsorption energy

The adsorption energy is calculated as the difference between the total energy of the full system and the energies of the isolated components,

$$E_{\rm ads} = E_{\rm tot} - (E_{\rm HA} + E_{\rm Mg}) \ . \qquad (1)$$

Here, $E_{\rm tot}$ is the total energy of HA adsorbed on the Mg surface after full structural relaxation. The surface reference energy $E_{\rm Mg}$ is calculated for the clean or doped Mg surface, depending on the system. The reference energy of HA, $E_{\rm HA}$ is obtained at the lateral lattice constants that fit the Mg(0001) surface and allowing the atomic positions to relax.

D. Hydroxyapatite

HA has the stoichiometric formula $Ca_{10}(PO_4)_6(OH)_2$ in a hexagonal bulk unit cell (space group $P6_3/m$), with 44 atoms per unit cell. We obtain the structure from Materials Project [64] but further relax the lattice constants and atomic positions using the vdW-DF-cx functional. Bulk HA has a layered structure, for which we find in-plane (vertical) lattice constant a = 9.415 Å (c = 6.868 Å), in excellent agreement with values from experiment [65] a = 9.43 Å and c = 6.88 Å. The in-plane lattice constant is approximately three times that of Mg(0001), for HA coating on Mg we therefore use one layer of HA on 3×3 Mg(0001), thus stretching HA approximately 2% to fit the underlying Mg surface.

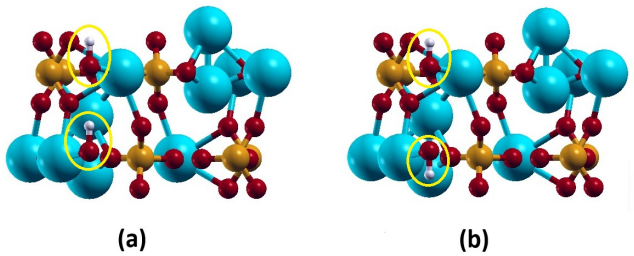

FIG. 2. HA structures with OH group orientations (a) as energetically favoured for a single layer of HA (b) as in bulk HA. The two OH groups in each panel are marked with yellow circles. Atom colors as in Figure 1.

The two hydroxyl groups in a HA layer in bulk align along the c-axis, Figure 2(a), creating a net dipole. However, as we describe in the Results section, when a single layer of HA is isolated, it is energetically favourable to have both H atoms pointing outward, thus flipping one OH group, as illustrated in Figure 2(b). We therefore use this structure for the coating adsorption studies presented here.

E. Zinc or calcium alloying of Mg(0001)

To investigate the effect of sparse Zn or Ca alloying of Mg(0001), one Mg atom in the surface top layer of Mg(0001) is substituted in the 3×3 supercell. This corresponds to a Zn (Ca) concentration of 5.8 wt% (3.6 wt%) of the atoms in the two exposed layers of Mg. Several structures were constructed with varied dopant positions in the top layers, relative to the HA coating, in order to explore how the position of the alloying atom may influence the interaction. The positioning of the substitutes was determined based on the optimal placement of HA over pristine Mg(0001). Each dopant position was selected to examine interaction with a given HA atom or with no HA atom specifically targeted.

The position of each Mg top layer atom within the 3×3 supercell is designated by an index notation (n, m), where (0,0) corresponds to the lowest left-hand corner of the supercell, Figure 3. The selected sites for substitution, Fig. 3(b), are position (2,0), which is located beneath a hydrogen (H) atom of a -OH group, position (0,2) underneath a Ca atom, position (0,1), located close

View Article Online
DOI: 10.1039/D6CP01070A 4

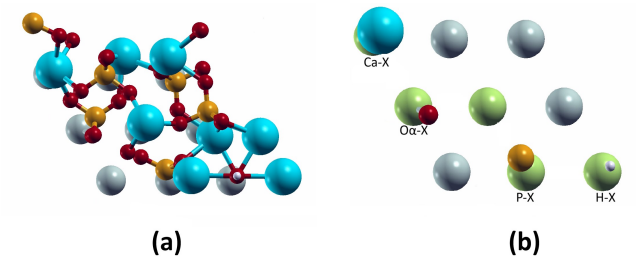

FIG. 3. Atomic configurations showing the positions of the substituted atoms. (a) All of HA above the top layer of Mg. (b) Substituted atom positions in green and including only the atoms in HA that are directly above them. Notation Ca-X means HA-bound Ca atom over substituted atom X (Zn/Ca). Only one Mg atom at a time is substituted. Other atom colors as in Figure 1.

to an oxygen (O) atom, position (1,1) at the center of the structure and not under any particular HA atom, and finally position (1,0), which is located underneath a phosphorus (P) atom.

IV. RESULTS AND DISCUSSION

A. Hydroxyapatite on pristine Mg(0001)

HA in the bulk structure has both OH groups pointing in the same direction, Figure 2(a), but for a single layer of HA we test and find that a structure with both H atoms pointing out of the layer, Fig. 2(b), is energetically favored: the gain in energy for the H-out structure is 9.9 meV/Å^2, or 0.79 eV per flipped OH group, compared to the structure with both H atoms pointing the same direction. We also test the structure with both H atoms pointing into the layer, and find that the cost, again compared to having the H atoms in the same direction, is 7.0 meV/Å^2, or 0.56 eV per flipped OH group. We therefore use the structure with H-atoms out, Fig. 2(b), for our analysis of a single HA layer as coating on Mg(0001).

As part of the analysis we determine the energy cost of cleaving the bulk into separate, single layers of HA. Keeping the lateral lattice constant ($a = 9.415$ Å) the same as in bulk, this cost is 91.9 meV/Å^2 for each interface that is broken, with local atomic positions relaxed but the OH groups still pointing in the same direction. Compared to a free HA layer with both OH groups pointing out of the layer and optimal (for that situation) lateral lattice constant $a = 9.264$ Å the cost reduces to 85.9 meV/Å^2.

The optimal positioning of the HA coating layer relative to the Mg surface was investigated by systematically translating the HA layer across the Mg surface. Within one unit cell of Mg(0001) a total of 25 equally distributed positions were evaluated. In each such position we allowed all atoms of the HA layer to relax in the direction perpendicular to the surface but not laterally, to keep the HA layer from "sliding" off unfavorable positions, and the atoms of the two top layers of the Mg surface were allowed to move in all directions. This approach enables identification of the energetically most favorable adsorption site by sampling a representative range of positions across the Mg surface.

Figure 4 shows the PES based on the 25 calculated positions with restraints on HA atomic lateral positions. The region calculated is highlighted with a red rectangle, values outside the rectangle are periodic copies. The plot indicates that there is a preferred adsorption site for HA over the Mg surface. However, the calculated energy difference between the optimal and the energetically worst position is relatively small, at 9.9 meV/Å^2, which is only double the energy required to slide a graphene layer on a surface of graphite [62]. This suggests that the corrugation of HA on Mg(0001) is small, as also seen for a layer of magnesiumhydroxide ($Mg(OH)_2$) on Mg(0001) [62] and discussed more for DFT-calculations of chloroform on graphene in Ref. [66].

After further relaxation of all atoms at the optimal adsorption site, the system converges to $E_{ads} = -14.4$ meV/Å^2 for HA on pristine Mg(0001).

Due to the low corrugation of HA on pristine Mg(0001) a HA layer may thus slide across the Mg surface rather easily. This could happen, for example, if a small force is applied, or to allow for the HA layer to adsorb non-stretched in large patches on the Mg surface and thus with the majority of the HA-Mg(0001) interface in other relative positions than the optimal. If the Mg surface develops cracks or irregularities the HA layer can also accommodate these at a low cost by locally adsorbing in less-than-optimal positions, without necessarily also developing cracks in the HA layer. This mobility can help release stress between the interface of HA and Mg, lowering the risk of holes or cracks appearing in the HA layer.

As reference for the adsorption energies we use a free-standing HA layer with the same lateral lattice constant as 3×3 Mg(0001), OH groups pointing out, and with relaxed atomic positions. If we instead were to use as the reference either a free-standing layer of HA (with the smaller optimized lattice constant $a = 9.264$ Å and the OH groups pointing out), or a layer of HA in its bulk (at lateral lattice constant $a = 9.415$ Å and with OH groups pointing the same direction) the reported adsorption energies would include the cost of stretching the free-standing layer from its smaller optimized lattice constant (cost 10.3 meV/Å^2), or the cost of first "cutting" out the HA layer from bulk and then stretching it (at a cost 93.4 meV/Å^2, including the gain of flipping one OH group once isolated from bulk). While we do not explicitly include these energy costs, they can easily be added to all adsorption energies provided in this study, if of relevance.

Given the smaller optimal lattice constant for the free-standing or bulk-situated HA layer and the relative ease with which HA can slide on the Mg surface, it is possible that in large patches of HA on Mg, the HA structure will shrinks in size in relation to the Mg surface, to approach

View Article Online
DOI: 10.1039/D6CP01070A 5

these smaller lattice constants. We can use the PES in Figure 4 to estimate the adsorption energy per area in a large, un-stretched patch of HA on Mg(0001): Each unit of HA will be offset an increasing distance from the optimal position, and we can estimate the contribution to the adsorption energy for each such unit from the PES plot. Doing so, we find that the adsorption energy averaged over a large patch will increase (become worse) by 4.5 meV/Å^2, compared to the stretched HA on Mg(0001), not counting the energy that goes into stretching the HA layer.

While the current study focuses on building one layer of HA on Mg(0001), either as a coating or spontaneously assembled from molecules and atoms in the body environment, the build up of multiple layers could also be envisioned. To study this, we calculated the adsorption energy of a second HA layer on top of an already adsorbed HA layer, both layers stretched. The layer near the Mg surface has the two OH groups pointing out from the layer (as in all our other adsorption results), while the top HA layer has both OH groups pointing away from the Mg surface, to mimic the HA-HA interface in bulk. Under these conditions the second HA layer adsorbs on HA-Mg(0001) with adsorption energy −83.5 meV/Å^2 relative to a single HA layer on Mg and an isolated, stretched HA layer with OH groups pointing out (as for all our adsorption energies). This adsorptio is clearly stronger than for a HA layer adsorbed directly on Mg(0001), and similar to the energy discussed earlier, of splitting HA bulk into layers.

However, for a given amount of HA available, a full one-layer HA coverage should be compared not just to a two-layer coverage, but to, e.g., 50% of a two-layer covered Mg surface and 50% of uncovered Mg surface. Such comparison shows that two-layer patches combined with clean Mg areas are still favorable over a full single layer adsorption, by 34.7 meV/Å^2. This energy does not include the cost of breaking a HA layer vertically to obtain the boundaries of the patches, a cost that will heavily depend on which and how many bonds within HA will be broken, each presumably at a relatively high cost of energy because those bonds are covalent, rather than the weaker binding between layers of HA. Thus, while it is in principle possible with multilayer patches, the energetics will depend also on the complex body environment and the details of the patches, factors that we cannot include in the present study. Further, the uncovered parts of the Mg surface will then likely be covered by other compounds, such as beginning oxides [32], magnesiumhydroxides [62], or smaller molecules such as amino acids [61]. We therefore refrain from predicting whether the adsorption is more likely to be a full single layer of HA, or patches of multilayers next to uncovered areas of Mg. Notwithstanding, we believe our results, in particular the local atomic positions and electron density changes, can form valuable input to further studies using larger-scale models, as these results are local to the HA-Mg interface and are not expected to change at thicker coverages of

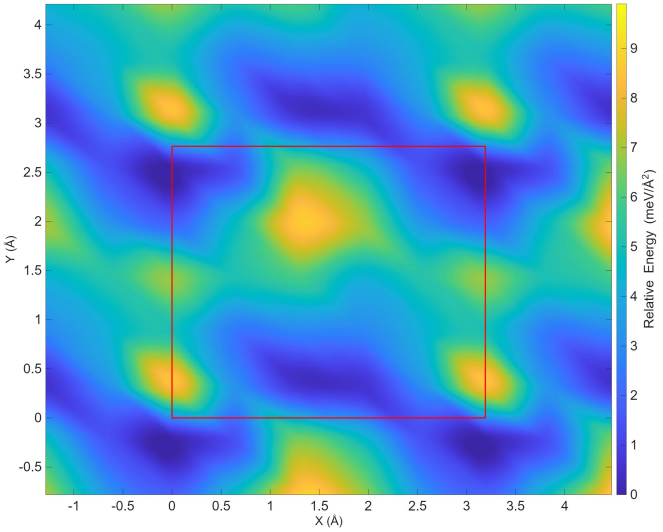

FIG. 4. Potential energy plot for relative position of HA on Mg(0001), for estimating the optimal positioning of HA over the Mg surface. Energies relative to the energy of the optimal position.

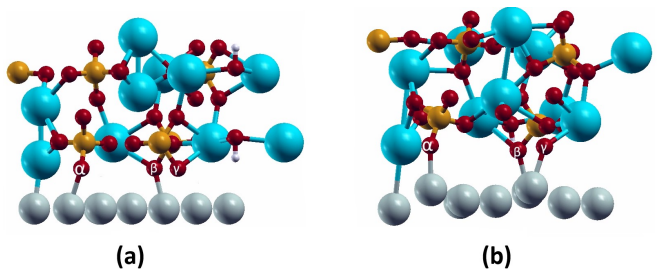

FIG. 5. Structural changes of HA in the optimal position, starting from (a) the structure of an isolated layer of HA (slightly stretched in the lateral directions) and clean Mg(0001) brought together at 2 Å separation, and (b) after optimization of the atomic positions. Atom colors as in Figure 1.

HA (and do not change noticeable after adsorption of a second layer of HA).

Focusing now on the stretched HA in the optimal position on Mg(0001), we see in Fig. 5 that the Mg atom positioned beneath the lowest Ca atom of HA moves slightly downward, away from HA, relative to the Mg surface without adsorbed HA. Meanwhile, three Mg atoms situated beneath or near the lowest O atoms in HA (marked by α, β and γ) move towards the O atoms. The top part of Table I summarizes the distances between these atoms, while the middle part of Table II (line HA-Mg) summarizes the vertical changes of a selection of the Mg atoms relative to their positions *before* HA adsorption, quantifying the findings in Fig. 5: the Mg atoms in positions (1,0) and (0,1) move outwards, toward the lowest HA O atoms, and inwards in position (0,2), away from the lowest HA Ca atom. The other top-layer Mg atoms selected

View Article Online
DOI: 10.1039/D6CP01070A 6

TABLE I. Changes in distances between pairs of atoms in the alloyed Mg surface and HA, relative to the structure of HA on pristine Mg(0001) shown in Figure 5(b). The changes are given in Δx, Δy and Δz, and the change in the length of the distance vector, $\Delta r = |\mathbf{R}_{\rm relax}| - |\mathbf{R}_{\rm prist}|$. Positive (negative) values signify that the distance in that direction between the two atoms has increased (decreased). Also shown is the distance between atoms after the relaxation, $R_{\rm relax} = |\mathbf{R}_{\rm relax}|$, where $\mathbf{R}_{\rm relax}$ is the distance vector for the two atoms for HA on either pristine Mg(0001) (then same as $\mathbf{R}_{\rm prist}$) or on alloyed Mg. Values are for pristine Mg(0001) (top of table), for alloying with Ca (middle part of table), and for alloying with Zn (lower part of table). For the latter two the alloying atom is placed beneath the HA atom mentioned. All values in Å.

Doping	Atom pair	Δx	Δy	Δz	Δr	$R_{\rm relax}$
	Ca-Mg	-	-	-	-	3.085
	O_α-Mg	-	-	-	-	2.088
	O_β-Mg	-	-	-	-	2.032
	O_γ-Mg	-	-	-	-	2.053
(0,2)	Ca-Ca	0.281	0.297	−0.148	−0.102	3.186
(0,1)	O_α-Ca	−0.118	−0.039	−0.138	−0.154	2.253
(1,0)	P-Ca	0.050	−0.067	−0.137	0.139	3.439
(2,0)	H-Ca	0.406	−1.341	0.852	0.409	2.484
(0,2)	Ca-Zn	−0.004	0.152	0.140	0.156	2.929
(0,1)	O_α-Zn	−2.278	0.073	−0.637	−1.598	3.698
(1,0)	P-Zn	−0.217	−1.246	−0.682	−0.912	4.212
(2,0)	H-Zn	0.117	−0.037	−0.018	0.010	2.883

in Figure 3 do not move much.

All three O-Mg pairs, listed in the top part of Table I, end up with a similar separation $R_{\rm relax}$, at about 2.05 Å, which is slightly smaller than the out-of-plane Mg-O separation (2.004 Å [24]) in the wurtzite (WZ) phase of MgO, as found using calculational settings very similar to the present ones. WZ-MgO is the first (metastable) phase that appears in the top of Mg(0001) as oxidation starts [32], while the final, stable rock salt phase has a longer Mg-O separation (2.115 Å [24]). The Ca-Mg pair shows a separation of about 3.1 Å, which is 0.1-0.8 Å smaller than the Mg-Mg or Ca-Ca distances calculated in their respective hcp phases [61]. These displacements show that the surface atoms of Mg are influenced by both the Ca atom and the O atoms of the HA layer, leading to a rearrangement in the Mg surface as seen in Fig. 1, with compressed Mg-Ca bonds and slightly stretched Mg-O bonds. However, as seen from the PES plot (in which these out-of-plane relaxations are included) this does not change the adsorption energy in any major way, as the difference in adsorption energy across the surface is only 9.9 meV/Å^2, with these relaxations included.

B. Alloying of Mg(0001)

When one of the Mg atoms is substituted by a Zn or Ca atom the positions of the atoms in the surface change. For Zn alloying, Zn dips into the surface, and Ca moves partly out of the surface, as already seen in Ref. [61] for the same calculational conditions, but in a 5×5 surface unit cell, while we here use a 3×3 surface cell. For the present surface unit cell, the upper part of Table II shows the displacement along the z-direction of the dopant atom compared to the position of the Mg atom it replaces.

In this smaller surface unit cell we find that the vertical changes in position of the Zn and Ca atoms, compared to the position of the Mg atom that they replace, is −0.34 Å (into the surface) for Zn and +0.57 Å (out of the surface) for Ca, top of Table II, in good agreement with the results of Ref. [61] in the larger surface cell. Due to its larger atomic radius, the Ca atom does not fit into a Mg lattice, which explains why it is pushed out of the surface. In contrast, Zn has an atomic radius a bit smaller than that of Mg and therefore integrates more favorably into the Mg lattice and is even dragged further into the surface to have smaller distances to the second layer Mg atoms.

C. Adsorption of hydroxyapatite on alloyed Mg(0001)

The adsorption energies of HA on pristine and alloyed Mg(0001) are summarized in the bottom part of Table II. These show that the position of the alloying atom, whether Zn or Ca, matters for the stability of the system. The energetically most favorable position for Ca is (1,1), under a void in HA, with HA adsorption energy −21.2 meV/Å^2, whereas position (0,1), under atom O_α, provides the most favorable configuration for Zn at −22.4 meV/Å^2. In general, the stability of both systems varies with the position of the substituted atom, and the adsorption energy can be either stronger or (in some cases) less strong than HA on a pure Mg surface, −14.4 meV/Å^2.

We calculate the atom positions in the interface between HA and the Mg surface after adsorption of a HA layer and compare to (i) positions when HA is adsorbed on pristine Mg(0001), Table I; and to (ii) positions of the alloying atom and the Mg atom positions before adsorption of a HA layer, Table II. From the first comparison we learn how the alloying affects the interface, and from the second comparison we learn how the Mg surface, whether pristine or alloyed, is affected by the adsorption of a HA layer.

Zn doping. Before adsorption of a HA layer, Zn takes a position in the Mg(0001) surface that is further into the surface than that of the Mg atom it substitutes. With adsorption of a layer of HA on the already alloyed Mg surface, the largest change is that Zn at position (0,2), under the lowest HA Ca atom, moves 0.15 Å further into the surface, Table II row HA-Mg(Zn), and ends up at a height −0.49 Å relative to the Mg atom in pristine Mg(0001) without HA adsorption, seen by adding the distance found in Table II row Mg(Zn).

View Article Online
DOI: 10.1039/D6CP01070A

The data for Zn alloying in Table I, bottom part, shows that substituting Zn into the Mg surface changes the relative atomic positions of Zn and the Ha atoms in all directions, relative to pristine Mg(0001) with HA. This is most pronounced for Zn in position (0,1), that is, under O_α before alloying, and for Zn under P, position (1,0); compare also Figure 5(b) before alloying to Figure 7 top panels (0,1) and (1,0) after alloying. There is clear repulsion of O from Zn, or rather, attraction to a Mg atom neighboring the Zn atom. This is because substitution with Zn in Mg(0001) changes the electron structure of the neighboring Mg atom to become more attractive for O adsorption [61].

In general, however, the substitution of a Zn-atom in the top layer of Mg(0001) does not seem to have any major structural effect in HA or the surface.

Ca doping. Introduction of a Ca alloying atom, compared to HA on pristine Mg(0001), shows a significant change when this Ca atom is placed in a position underneath a void in the HA layer, at position (1,1), Figure 6 bottom right. Placed in that position, the Ca dopant atom moves further away from the Mg surface than in Mg(0001) without HA (compare Table II rows Mg(Ca) and HA-Mg(Ca)) and into the HA structure. Since Ca is one of the main atoms in HA, it is reasonable that a Ca atom in Mg(0001) tends to move closer into the HA layer if there is space available, reflecting its natural affinity for the HA structure. The alloy Ca atom then enters the HA layer into a position that is almost a mirror image of the Ca atom furthest up in the HA layer, and is a position similar to that of a Ca atom in stacked HA layers such as in a HA bulk-like scenario. This position is also energetically favored, Table II bottom. We confirmed this scenario by a calculation of three HA layers. There, the highest Ca atom in a lower layer was found to merge into the layer above, while still remaining part of the HA layer. The Ca alloy atom at the HA-Mg interface moves further, and separates from the Mg surface, leaving a vacancy in the Mg surface.

Generally, for the systems considered here, the Ca alloy atom tends to move away from the Mg surface, both relative to the position of Ca in Mg(0001) without adsorbed HA, and relative to the Mg atom which it replaces in the HA-on-pristine-Mg situation. This is likely due a combination of the larger size of the Ca atom compared to Mg, and the attraction to the O atoms in HA, and more generally the HA environment where Ca atoms are already present.

The exception among the systems, with Ca moving into the surface instead of out, is the alloy Ca atom placed directly under a low Ca atom in HA, position (0,2), where the two Ca atoms experience repulsion. There, the alloy Ca atom is positioned at 0.57 Å above the Mg surface when no HA is present, but changes to a position 0.80 Å lower when HA is adsorbed, at vertical position $-0.80 + 0.57 = -0.23$ Å (Table II), i.e., the alloy Ca atom moves into the Mg surface due to the repulsion from the Ca atom in HA directly above. However, even though the two Ca atoms experience repulsion, the surrounding Mg and HA structure approximately maintain their positions and prevent the HA layers from moving further away from the Mg surface. The Ca-Ca distance (Table I) is here 3.186 Å, which is smaller than the Ca-Ca distance 3.95 Å in the stable face-centered cubic bulk structure. This competition comes at a cost, energy wise: Position (0,2) has the weakest adsorption energy of all the studied situations, at -5.2 meV/Å^2.

TABLE II. Atom positional changes and adsorption energies of HA on Mg surfaces. Displacements are measured along the z-direction in Å, adsorption energies in meV/Å^2. The change in vertical position of Zn or Ca in Mg(0001) without HA, relative Mg atoms in pristine Mg(0001), are given in the top part of the table, these are the reference points for displacements upon adsorption of HA (middle part).

Position	(0,1)	(0,2)	(1,0)	(1,1)	(2,0)
No HA, displacement relative pristine Mg(0001)					
Mg(Zn)	−0.34	−0.34	−0.34	−0.34	−0.34
Mg(Ca)	0.57	0.57	0.57	0.57	0.57
With HA, displacement relative to no HA					
HA–Mg	0.54	−0.38	0.63	−0.01	−0.12
HA–Mg(Zn)	−0.03	−0.15	−0.06	0.09	0.06
HA–Mg(Ca)	−0.01	−0.80	0.08	1.37	0.33
Adsorption energy of HA on Mg(0001)					
HA–Mg	−14.4	−14.4	−14.4	−14.4	−14.4
HA–Mg(Zn)	−22.4	−19.8	−14.2	−15.3	−16.5
HA–Mg(Ca)	−20.0	−5.2	−20.7	−21.2	−12.7

Nominally, in the position (2,0) the H-to-alloy-Ca distance increases, Table I bottom part, compared to the case with pristine Mg(0001). At the same time, the alloy Ca atom moves further out of the Mg surface by 0.33 Å (Table II) once the HA is adsorbed. This is because the O atom in the -OH group, of which the H atom is a part, becomes available for binding to the alloy Ca, and this pushes the H atom out of the way, as seen in Fig. 7 bottom, leading to a larger alloy-Ca-to-H distance. Again, moving the H atom comes at a cost: the adsorption energy for the (2,0) situation is -12.7 meV/Å^2, weaker than without the alloying and weaker than most of the alloying positions considered here.

To sum up, for HA adsorbed on Ca-alloyed Mg(0001), most of the relative positions show more favorable adsorption than on pristine Mg(0001). The relative positions studied here have adsorption energies that range from -5.2 to -21.2 meV/Å^2, indicating that the corrugation for HA on Ca-alloyed Mg(0001) is larger with Ca alloying than without. The HA sheet will thus not be as mobile on the Mg surface as on pristine Mg. HA adsorption on Zn-alloyed Mg, on the other hand, shows less differences in adsorption energies and a corrugation estimated to be similar to that of HA on pristine Mg(0001) (estimated from the -14.2 to -22.4 meV/Å^2 adsorption energies found in the systems studied here). The stabil-

View Article Online
DOI: 10.1039/D6CP01070A 8

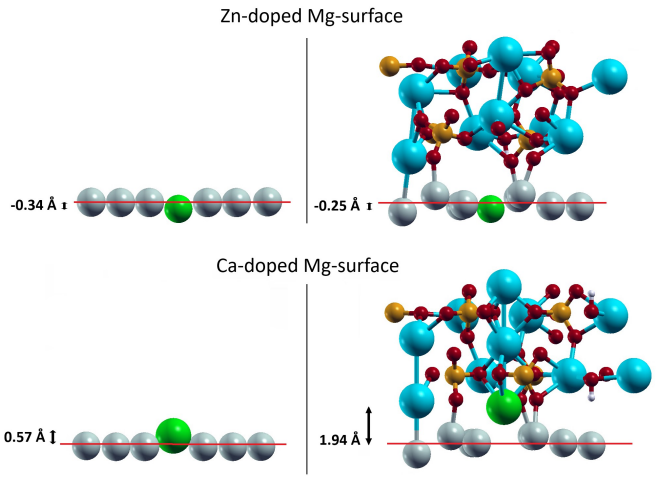

FIG. 6. *Left:* Mg(0001) with a doped atom substituted at position (1,1). *Right:* Same surface but relaxed with HA. Green atoms indicate substituted atoms. The red reference lines indicate the position of Mg atoms in pristine Mg(0001) without HA. Atom colors as in Figure 1.

ity of a HA layer on Zn-alloyed Mg therefore seems to be similar to that of HA on pristine Mg.

Our calculations have alloying atoms placed sparsely but periodically repeated, due to the periodic boundary conditions in our calculations. As such, the systems we calculate can be seen as motifs for the adsorption. Real systems, with the solid-solution alloy atom have a distribution of ally atoms that is not periodic, and over areas of large HA flakes on the surface, the adsorption energy will be a weighted average of the values found here.

D. Electron density

To better understand the interaction between HA and the Mg surface, electron density plots were generated for the optimized structures, analyzing the interface for both pure and doped Mg(0001). Changes in the electron density are evaluated similarly to the adsorption energy, but without any additional structural relaxation calculations when HA and surface are pulled apart: The electron density of the combined system is compared to the sum of the electron densities of the isolated but still deformed HA layer and Mg surface. In Figures 8-10 we thus plot the electron density difference due to the adsorption of the HA layer. Isolines have separation $7 \cdot 10^{-4}$ a.u. (electrons/Bohr^3), and the color scale goes from $5 \cdot 10^{-3}$ a.u. (red, increased electron density) to $-5 \cdot 10^{-3}$ a.u. (blue, decreased electron density).

Changes in electron density for HA adsorption on pristine Mg is visualized in Figure 8. The largest electron accumulations are near the three O-atoms (O_α, O_β and O_γ) that are close to the Mg atoms, and between the lowest Ca atom in HA and a Mg atom. Meanwhile, electron depletion is also seen around the Mg atoms and above the

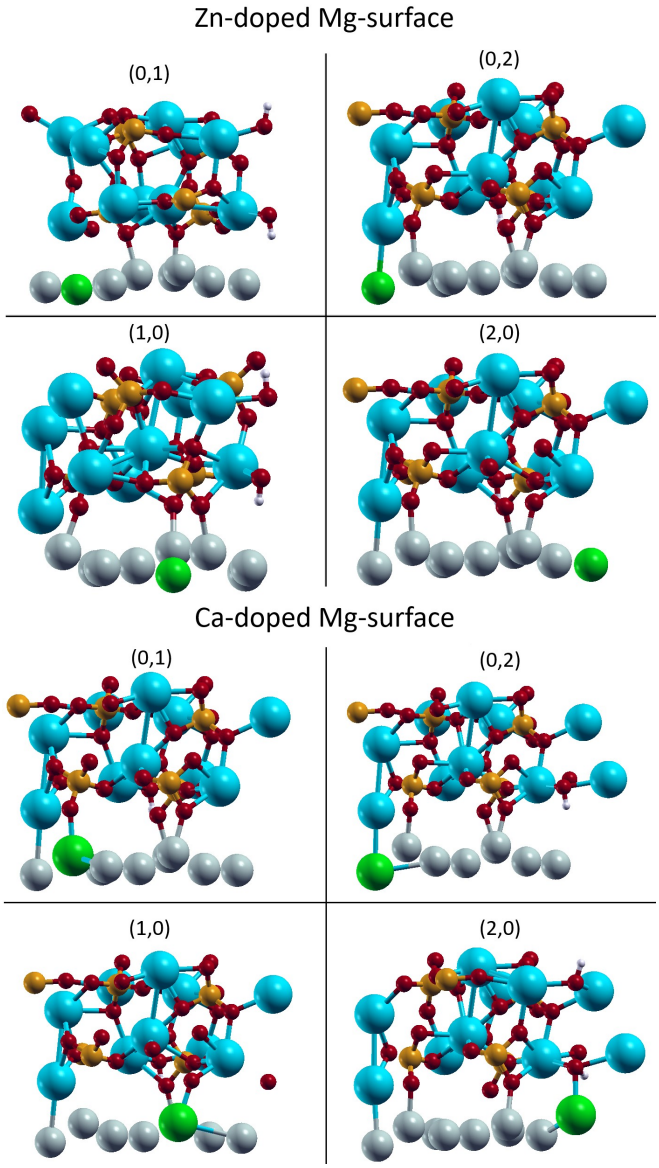

FIG. 7. Optimized structures for Ca and Zn substitution at position (0,1), (0,2), (1,0) and (2,0). Green atoms indicate substituted atom, in the top part a Zn atom, in the bottom part a Ca atom. Other atom colors as in Figure 1.

O atoms in the directions to other atoms. We use these to compare to the cases with HA on Ca- or Zn-alloyed Mg in the following figures.

Figure 9 shows the Ca-doped system, with focus on the positions of the Ca alloying atom in the five positions examined, Fig. 3(b). With Ca in position (1,1), top panels of Fig. 9, the maximum electron density change is $3.6 \cdot 10^{-2}$ a.u. This is larger than for any of the other systems. We know from the structural changes illustrated in Figure 6 that when Ca is placed in position (1,1) the atom moves into the HA layer to a spot surrounded by three O atoms (marked by numbers 1, 2, and 3 in Figure 9). These O atoms are positioned further into the

View Article Online
DOI: 10.1039/D6CP01070A 9

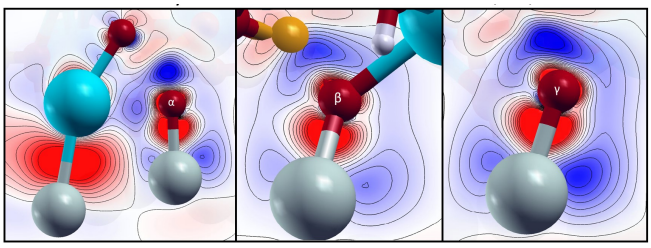

FIG. 8. HA over pure Mg(0001); Change in electron density with red (blue) regions marking addition (depletion) of electron density, and isoline differences $7 \cdot 10^{-4}$ a.u. Changes near the lowest Ca atom and the three O atoms marked α, β and γ in Figure 1. Atom colors as in Figure 1.

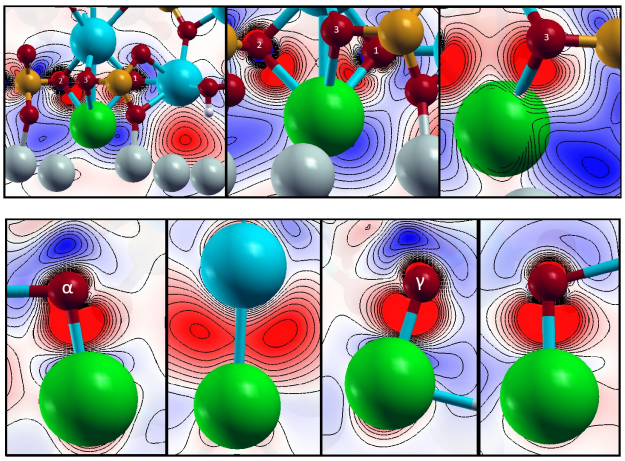

FIG. 9. Change in electron density for HA adsorbed on the Ca-doped Mg surface. Isolines separated by $7 \cdot 10^{-4}$ a.u. *Top*: Ca atom at position (1,1), overview (left) and zoomed in on parts of the structure (middle and right). *Bottom*: Ca in positions (0,1), (0,2), (1,0), and (2,0) (from left to right). The H atom in (2,0) has moved and made the O atom in the -OH group available for interaction with the Ca atom. Atom colors as in Figure 1 and with the Ca alloying atom in green.

HA layer than the O atoms marked by α, β and γ in previous figures. Given the high reactivity of O and its strong tendency to attract cations, it is reasonable that Ca stabilizes in a position close to these O atoms and consistent with the electron accumulation between the alloy Ca atom and the O atoms with labels 1, 2, and 3.

The other examined interfaces of HA with Ca-doped Mg(0001) are shown in the bottom panels of Figure 9. The electron accumulation between the alloy Ca atom and the HA Ca atom, position (0,2), is more delocalized compared to the interaction between Ca and O. This is to be expected because Ca atoms have low electronegativity, neither of the Ca atoms attract the excess electron density strongly to localize it between them, leading to two lobes on each side instead of a single lobe in the middle. Meanwhile, the alloy Ca atom and O in HA shows a typical interaction between an electronegative and electropositive atom in the three other bottom panels, for Ca alloy positions (0,1), (1,0) and (2,0). Thus, O strongly attracts electron density whereas Ca donates electron density from its outer shell, leading to the localized lobe rather than the more delocalized pattern observed between the two Ca atoms.

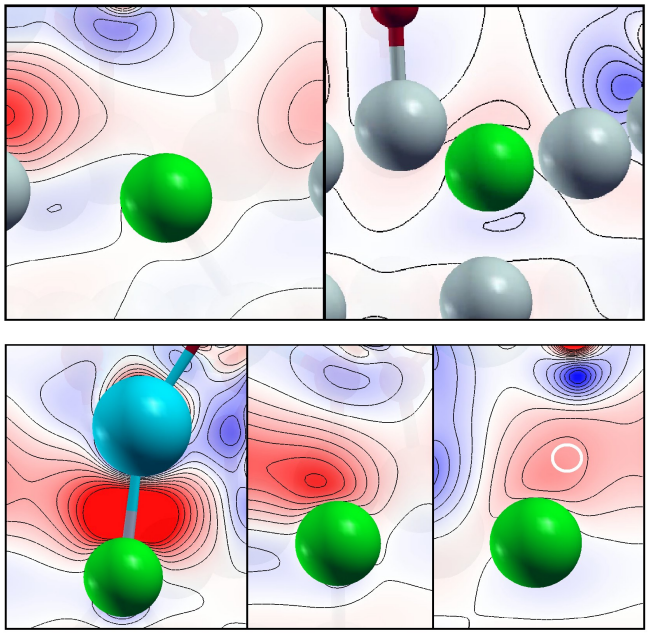

FIG. 10. Change in electron density for HA adsorbed on the Zn-doped Mg surface. Isolines separated by $7 \cdot 10^{-4}$ a.u. *Top*: Zn atom at position (0,1) (left) and (1,1) (right); *Bottom*: Zn atom at positions (0,2), (1,0), and (2,0) (left to right). In the panel for (2,0) a H atom is slightly behind the plane of the panel and its position is marked by a white circle. Atom colors as in Figure 1, and Zn in green.

In the HA interfaces with the Zn-doped surfaces, Figure 10, the electron density changes are smaller than in the other systems. As seen in the middle row of Table II the Zn-atom does not move much when HA is adsorbed on the already alloyed Mg surface. This is reflected in the electron density changes: There is very little electron accumulation between Zn and neighboring atoms in position (0,1) (O neighboring atom) and (1,1) (mostly Mg atoms nearby), and in position (0,2) the Zn to Ca interaction shows the largest electron accumulation among the Zn-doped systems, but still smaller than in most of the systems with Ca-alloyed or pristine Mg(0001). In position (1,0) the Zn atom has P, Ca and some O atoms as nearest neighbors but at a distance such that the electron changes that these give rise to are spread out. Finally, in position (2,0) the H atom above Zn is out of the vertical plane that goes through Zn, and the position of the H atom is indicated by the white circle in the panel. There, we see some low level electron accumulation.

The electron density change plots overall show larger variation for HA on Ca doped surfaces than for HA on Zn doped surfaces. This is in agreement with the differences in adsorption energy being larger for HA on Ca doped

View Article Online
DOI: 10.1039/D6CP01070A

surfaces than on Zn doped surfaces.

V. SUMMARY

We investigated the interaction of one layer of HA with pristine and doped Mg(0001), where for the doping we used one Zn or Ca atom to replace one out of 18 exposed Mg atoms in a 3×3 Mg(0001) surface cell. Our calculations show that HA binds to the Mg surface but that the interaction is relatively weak, with an adsorption energy of -14.4 meV/Å^2 on pristine Mg(0001) and between -5.2 and -22.4 meV/Å^2 on doped Mg(0001), depending also on the relative position of the dopant and the HA layer.

For HA on pristine Mg(0001) we studied the corrugation by calculating the PES from a set of adsorption energies at positions distributed on the surface. We found that also the corrugation is low, with 9.9 meV/Å^2 as the difference between the energetically worst and best adsorption position. Thus the energy cost of HA sliding across the pristine Mg surface is low.

In the calculations we stretch the HA layer 2% to fit it onto the 3×3 surface unit cell of Mg(0001). Using the PES plot we estimate the additional cost of having large patches that are not stretched and thus cannot sit in optimal positions in all parts of the patches. We find that this changes the adsorption energy by about 4.5 meV/Å^2, not including the energy difference between a stretched and non-stretched isolated HA layer.

Doping the Mg surface with Ca or Zn affects the interaction with HA. Ca-doped surfaces show a variation of stability and deformations in the HA-Mg interface, with the best adsorption energy in a situation where the Ca atom leaves the Mg surface and enters the HA layer. This leads to larger corrugation than on pristine Mg. Zn-doped surfaces do not show any major deformations at HA adsorption, but still have better adsorption energy for HA than the pristine Mg surface.

Plots of the changes in electron density upon adsorption of HA show that the changes occur mainly between the lowest O atoms of HA and the Mg surface or the Ca atom of the doped surface, with electron accumulation near the O atoms, while there is less electron accumulation between the O atoms and Zn. Further, we find relatively large electron density changes between the lowest Ca atom of HA and the Mg, Ca or Zn atom in the Mg surface below it.

We believe that the results that we present here for the HA-Mg interface, on the electronic and atomic scale, are important for future studies in the materials science community in larger-scale models, for which our current results can act as non-empirical model parameters.

AUTHOR CONTRIBUTIONS (CREDIT)

Anthony Veit Berg: Conceptualization (equal), Formal analysis (supporting), Investigation (lead), Visualization, Writing - original draft (equal). **Ablai Forster, Tim Hansson, Alex J. Jernstedt, and Emmy Salminen:** Conceptualization (equal), Investigation (supporting), Writing - review & editing. **Elsebeth Schröder:** Conceptualization (equal), Data curation, Formal analysis (lead), Funding acquisition, Investigation (supporting), Resources, Supervision, Validation, Writing - original draft (equal).

A.F., T.H., A.J., and E.S. (Emmy Salminen) contributed equally to this work.

CONFLICT OF INTERESTS

The authors have no conflicts of interests to disclose.

ACKNOWLEDGMENT

The present work is supported by the Swedish Research Council (VR) through Grant No. 2020-04997 and Chalmers Areas of Advance Nano and Materials. The computations were performed using computational and storage allocations from Chalmers Centre for Computational Science and Engineering (C3SE), and from the National Academic Infrastructure for Supercomputing in Sweden (NAISS), under contracts C3SE2025/1-6, C3SE2026/1-21, C3SE2026/1-23, NAISS2024/3-16, NAISS2024/6-432, NAISS2025/3-25, and NAISS2025/5-484.

DATA AVAILABILITY

Atomic coordinates are available within the supplementary material of the article.

[1] T. Kim, C. W. See, X. Li, D. Zhu, Orthopedic implants and devices for bone fractures and defects: Past, present and perspective, Eng. Regener. 1 (2020) 6–18. doi:10.1016/j.engreg.2020.05.003.

[2] V. Tsakiris, C. Tardei, F. M. Clicinshi, Biodegradable Mg alloys for orthopedic implants – A review, J. Magnes. Alloy. 9 (2021) 1884–1906. doi:10.1016/j.jma.2021.06.024.

[3] M. Niinomi, M. Nakai, Titanium-based biomaterials for preventing stress shielding between implant devices and bone, Int. J. Biomater. 2011 (2011) 1–10. doi:10.1155/2011/836587.

[4] B. J. Luthringer, F. Feyerabend, R. Willumeit-Römer, Magnesium-based implants: a mini-review, Magnes. Res. 27 (4) (2014) 142–154.

View Article Online
DOI: 10.1039/D6CP01070A

[5] D. Zhao, S. Huang, F. Lu, B. Wang, L. Yang, L. Qin, K. Yang, Y. Li, W. Li, W. Wang, S. Tian, X. Zhang, W. Gao, Z. Wang, Y. Zhang, X. Xie, J. Wang, J. Li, Vascularized bone grafting fixed by biodegradable magnesium screw for treating osteonecrosis of the femoral head, Biomaterials 81 (2016) 84–92. doi:10.1016/j.biomaterials.2015.11.038.

[6] H.-S. Han, S. Loffredo, I. Jun, J. Edwards, Y.-C. Kim, H.-K. Seok, F. Witte, D. Mantovani, S. Glyn-Jones, Current status and outlook on the clinical translation of biodegradable metals, Mater. Today 23 (2019) 57–71. doi:10.1016/j.mattod.2018.05.018.

[7] C.-W. Lin, C.-P. Ju, J.-H. C. Lin, A Comparison of the Fatigue Behavior of Cast Ti–7.5Mo with c.p. Titanium, Ti–6Al–4V and Ti–13Nb–13Zr Alloys, Biomaterials 26 (16) (2005) 2899–2907. doi:10.1016/j.biomaterials.2004.09.007.

[8] D. Noviana, D. Paramitha, M. F. Ulum, H. Hermawan, The effect of hydrogen gas evolution of magnesium implant on the postimplantation mortality of rats, J. Orthop. Transl. 5 (2016) 9–15. doi:10.1016/j.jot.2015.08.003.

[9] H. Ben Amara, J. Philip, O. Omar, P. Thomsen, Gas bubbles from biodegradable magnesium implants convey mechanical cues and promote immune cell stimulation, Adv. Sci. 12 (28) (2025) 2503123. doi:10.1002/advs.202503123.

[10] L. Guo, X. Zhang, Z. Zhang, Z. Hao, Degradation characteristics of high-purity magnesium implants under single static and cyclic compressive loads in vivo and in vitro, J. Magnesium Alloys 13 (4) (2025) 1480–1494. doi:10.1016/j.jma.2024.12.014.

[11] A. Mohamed, A. M. El-Aziz, H.-G. Breitinger, Study of the degradation behavior and the biocompatibility of Mg–0.8Ca alloy for orthopedic implant applications, J. Magnesium Alloys 7 (2) (2019) 249–257. doi:10.1016/j.jma.2019.02.007.

[12] D. S. Petrovič, D. Mandrino, B. Šarler, J. Horky, A. Ojdanic, M. J. Zehetbauer, D. Orlov, Surface analysis of biodegradable Mg-alloys after immersion in simulated body fluid, Materials 13 (2020) 1740. doi:10.3390/ma13071740.

[13] R. Willumeit, J. Fischer, F. Feyerabend, N. Hort, U. Bismayer, S. Heidrich, B. Mihailova, Chemical surface alteration of biodegradable magnesium exposed to corrosion media, Acta Biomater. 7 (2011) 2704–2715. doi:10.1016/j.actbio.2011.03.004.

[14] Y. Zhang, G. Zhang, M. Wei, Controlling the biodegradation rate of magnesium using biomimetic apatite coating, J. Biomed. Mater. Res. B 89 (1) (2009) 408–414. doi:10.1002/jbm.b.31228.

[15] H. Yang, X. Yan, M. Ling, Z. Xiong, C. Ou, W. Lu, In vitro corrosion and cytocompatibility properties of nanowhisker hydroxyapatite coating on magnesium alloy for bone tissue engineering applications, Int. J. Mol. Sci. 16 (3) (2015) 6113–6123. doi:10.3390/ijms16036113.

[16] M. E. Iskandar, A. Aslani, H. Liu, The effects of nanostructured hydroxyapatite coating on the biodegradation and cytocompatibility of magnesium implants, J. Biomed. Mater. Res. Part A 101A (8) (2013) 2340–2354. doi:10.1002/jbm.a.34530.

[17] S.-M. Kim, J.-H. Jo, S.-M. Lee, M.-H. Kang, H.-E. Kim, Y. Estrin, J.-H. Lee, J.-W. Lee, Y.-H. Koh, Hydroxyapatite-coated magnesium implants with improved *In Vitro* and *In Vivo* biocorrosion, biocompatibility, and bone response, J. Biomed. Mater. Res. Part A 101A (11) (2013) 3102–3112. doi:10.1002/jbm.a.34718.

[18] M. B. Kannan, Hydroxyapatite coating on biodegradable magnesium and magnesium-based alloys, in: M. Mucalo (Ed.), Hydroxyapatite (HAp) for Biomedical Applications, Woodhead Publishing Series in Biomaterials, Woodhead Publishing, 2015, pp. 289–306. doi:10.1016/B978-1-78242-033-0.00013-4.

[19] R. A. Dunne, D. E. Dickel, A. M. Green, D. Kim, L. B. Priddy, M. W. Priddy, Finite element and density functional theory modeling effectively predict pitting degradation of hydroxyapatite-coated pure magnesium, J. Biomed. Mater. Res. B 112 (12) (2024) e35519. doi:10.1002/jbm.b.35519.

[20] M. Geetha, A. K. Singh, R. Asokamani, A. K. Gogia, Ti based biomaterials, the ultimate choice for orthopaedic implants – A review, Prog. Mater Sci. 54 (3) (2009) 397–425. doi:10.1016/j.pmatsci.2008.06.004.

[21] W. Abd-Elaziem, M. A. Darwish, A. Hamada, W. M. Daoush, Titanium-based alloys and composites for orthopedic implants applications: A comprehensive review, Mater. Des. 241 (2024) 112850. doi:10.1016/j.matdes.2024.112850.

[22] N. Dehghan, N. Frane, A. Vohra, R. O'Connor, S. Deeyor, C. Hui, M. McKee, How difficult is titanium plate and screw implant removal? A retrospective case series, Injury 55 (11) (2024) 111824. doi:10.1016/j.injury.2024.111824.

[23] A. Kokalj, Computer graphics and graphical user interfaces as tools in simulations of matter at the atomic scale, Comput. Mater. Sci 28 (2) (2003) 155–168. doi:10.1016/S0927-0256(03)00104-6.

[24] Z. Xing, D. Orlov, E. Schröder, Tailored pseudopotentials for magnesium surface core level shift calculations, Phys. Rev. Mater. 8 (2024) 123801. doi:10.1103/PhysRevMaterials.8.123801.

[25] E. Schröder, R. Fasel, A. Kiejna, O adsorption and incipient oxidation of the Mg(0001) surface, Phys. Rev. B 69 (2004) 115431.

[26] Y. Li, P. Zhang, B. Sun, Y. Yang, Y. Wei, Atomic hydrogen adsorption and incipient hydrogenation of the mg(0001) surface: A density-functional theory study, J. Chem. Phys. 131 (3) (2009) 034706. doi:10.1063/1.3182851.

[27] Y. Li, Y. Yang, B. Sun, H.-Z. Song, Y. Wei, P. Zhang, Rotation of hydrogen molecules during the dissociative adsorption on the Mg(0001) surface: A first-principles study, Chin. Phys. B 19 (5) (2010) 058201. doi:10.1088/1674-1056/19/5/058201.

[28] M. Nezafati, K. Cho, A. Giri, C.-S. Kim, DFT study on the water molecule adsorption and the surface dissolution behavior of Mg alloys, Mater. Chem. Phys. 180 (2016) 16–22. doi:10.1016/j.matchemphys.2016.07.042.

[29] Z. Fang, J. Wang, S. Zhu, X. Yang, Y. Jia, Q. Sun, S. Guan, A DFT study of the adsorption of short peptides on Mg and Mg-based alloy surfaces, Phys. Chem. Chem. Phys. 20 (2018) 3602–3607. doi:10.1039/C7CP07431J.

[30] Z. Han, Y. Wu, H. Yu, S. Zhou, Location-dependent effect of nickel on hydrogen dissociation and diffusion on Mg(0001) surface: Insights into hydrogen storage material design, J. Magnesium Alloys 9 (2) (2021) 591–601. doi:10.1016/j.jma.2021.04.015.

View Article Online
DOI: 10.1039/D6CP01070A

[31] Z. Xing, M. Fanetti, S. Gardonio, E. Schröder, D. Orlov, Initial oxidation of low index Mg surfaces investigated by SCLS and DFT, Appl. Surf. Sci. 671 (2024) 160656.

[32] Z. Xing, D. Orlov, E. Schröder, Exploring the evolution of magnesium oxidation mechanisms by density functional theory, Surf. Sci. 761 (2025) 122806. doi:10.1016/j.susc.2025.122806.

[33] F. Fiesinger, D. Gaissmaier, M. van den Borg, J. Beßner, A. C. T. van Duin, T. Jacob, Development of a Mg/O ReaxFF Potential to Describe the Passivation Processes in Magnesium-Ion Batteries, ChemSusChem 15 (23) (2022) e202201821. doi:10.1002/cssc.202201821.

[34] D.-P. Ji, Q. Zhu, S.-Q. Wang, Detailed first-principles studies on surface energy and work function of hexagonal metals, Surf. Sci. 651 (2016) 1–10. doi:10.1016/j.susc.2016.04.007.

[35] Office of Dietary Supplements (ODS), Zinc, U.S. Department of Health and Human Services (2026).
URL https://ods.od.nih.gov/factsheets/Zinc-HealthProfessional/

[36] M. A. F. Romzi, J. Alias, M. I. M. Ramli, Effect of zinc (Zn) on the microstructure and corrosion behaviour of magnesium (Mg), Mater. Today Proc. 48 (Part 6) (2022) 1873–1879, elsevier. doi:10.1016/j.matpr.2021.09.261.

[37] H. R. Bakhsheshi-Rad, E. Hamzah, A. Fereidouni-Lotfabadi, M. Daroonparvar, M. A. M. Yajid, M. Mezbahul-Islam, M. Kasiri-Asgarani, M. Medraj, Microstructure and bio-corrosion behavior of Mg–Zn and Mg–Zn–Ca alloys for biomedical applications, Mater. Corros. 65 (2014) 1178–1187. doi:10.1002/maco.201307588.

[38] L. Xu, X. Liu, K. Sun, R. Fu, G. Wang, Corrosion behavior in magnesium-based alloys for biomedical applications, Materials 15 (7) (2022) 2613. doi:10.3390/ma15072613.

[39] NIH Office of Dietary Supplements, Calcium — health professional fact sheet (2025-07-11).
URL https://ods.od.nih.gov/factsheets/Calcium-HealthProfessional/

[40] Y. Wan, G. Xiong, H. Luo, F. He, Y. Huang, X. Zhou, Preparation and characterization of a new biomedical magnesium–calcium alloy, Mater. Des. 29 (10) (2008) 2034–2037. doi:10.1016/j.matdes.2008.04.017.

[41] Z. Li, X. Gu, S. Lou, Y. Zheng, The development of binary Mg–Ca alloys for use as biodegradable materials within bone, Biomaterials 29 (10) (2008) 1329–1344. doi:10.1016/j.biomaterials.2007.12.021.

[42] S. V. Dorozhkin, Calcium orthophosphates, J. Mater. Sci 42 (4) (2007) 1061–1095. doi:10.1007/s10853-006-1467-8.

[43] H. Shi, Z. Zhou, W. Li, Y. Fan, Z. Li, J. Wei, Hydroxyapatite based materials for bone tissue engineering: A brief and comprehensive introduction, Crystals 11 (2) (2021) 149. doi:10.3390/cryst11020149.

[44] I. Ielo, G. Calabrese, G. D. Luca, S. Conoci, Recent advances in hydroxyapatite-based biocomposites for bone tissue regeneration in orthopedics, Int. J. Mol. Sci. 23 (17) (2022). doi:10.3390/ijms23179721.

[45] M. Prakasam, J. Locs, K. Salma-Ancane, D. Loca, A. Largeteau, L. Berzina-Cimdina, Fabrication, properties and applications of dense hydroxyapatite: A review, J. Funct. Biomater. 6 (4) (2015) 1099–1140. doi:10.3390/jfb6041099.

[46] T. U. Habibah, D. V. Amlani, M. Brizuela, Hydroxyapatite dental material, statPearls [Internet]. Last updated 2022-09-12 (2022).
URL https://www.ncbi.nlm.nih.gov/books/NBK513314/

[47] M. Kauke-Navarro, L. Knoedler, S. Knoedler, A. F. Safi, Advancements in facial implantology: A review of hydroxyapatite applications and outcomes, Front. Surg. 11 (2024) 1409733. doi:10.3389/fsurg.2024.1409733.

[48] S. Mondal, S. Park, J. Choi, T. T. H. Vu, V. H. M. Doan, T. T. Vo, B. Lee, J. Oh, Hydroxyapatite: A Journey from Biomaterials to Advanced Functional Materials, Adv. Colloid Interface Sci. 321 (2023). doi:10.1016/j.cis.2023.103013.

[49] A.-M. Zhang, P. Lenin, R.-C. Zeng, M. B. Kannan, Advances in hydroxyapatite coatings on biodegradable magnesium and its alloys, J. Magnesium Alloys 10 (5) (2022) 1154–1170. doi:10.1016/j.jma.2022.01.001.

[50] R. I. M. Asri, W. S. W. Harun, M. Samykano, N. A. C. Lah, S. A. C. Ghani, F. Tarlochan, M. R. Raza, Corrosion and surface modification on biocompatible metals: A review, Mater. Sci. Eng. 77 (2017) 1261–1274. doi:10.1016/j.msec.2017.04.102.

[51] M. Tomozawa, S. Hiromoto, Y. Harada, Microstructure of hydroxyapatite-coated magnesium prepared in aqueous solution, Surf. Coat. Technol. 204 (20) (2010) 3243–3247. doi:10.1016/j.surfcoat.2010.03.023.

[52] M. Dion, H. Rydberg, E. Schröder, D. C. Langreth, B. I. Lundqvist, van der Waals density functional for general geometries, Phys. Rev. Lett. 92 (24) (2004) 246401. doi:10.1103/PhysRevLett.92.246401.

[53] K. Berland, P. Hyldgaard, Exchange functional that tests the robustness of the plasmon description of the van der Waals density functional, Phys. Rev. B 89 (2014) 035412. doi:10.1103/PhysRevB.89.035412.

[54] K. Berland, C. A. Arter, V. R. Cooper, K. Lee, B. I. Lundqvist, E. Schröder, T. Thonhauser, P. Hyldgaard, van der Waals density functionals built upon the electron-gas tradition: Facing the challenge of competing interactions, J. Chem. Phys. 140 (18) (2014) 18A539. doi:10.1063/1.4871731.

[55] E. Schröder, V. R. Cooper, K. Berland, B. I. Lundqvist, P. Hyldgaard, T. Thonhauser, Chapter 8 - The vdW-DF Family of Nonlocal Exchange-Correlation Functionals, in: A. Otero de la Roza, G. A. DiLabio (Eds.), Non-Covalent Interactions in Quantum Chemistry and Physics, Elsevier, 2017, pp. 241–274. doi:10.1016/B978-0-12-809835-6.00009-8.

[56] Quantum ESPRESSO, manifesto (May 2025).
URL https://www.quantum-espresso.org/manifesto/

[57] P. Giannozzi, S. Baroni, N. Bonini, M. Calandra, R. Car, C. Cavazzoni, D. Ceresoli, G. L. Chiarotti, M. Cococcioni, I. Dabo, A. D. Corso, S. Fabris, G. Fratesi, S. de Gironcoli, R. Gebauer, U. Gerstmann, C. Gougoussis, A. Kokalj, M. Lazzeri, L. Martin-Samos, N. Marzari, F. Mauri, R. Mazzarello, S. Paolini, A. Pasquarello, L. Paulatto, C. Sbraccia, S. Scandolo, G. Sclauzero, A. P. Seitsonen, A. Smogunov, P. Umari, R. M. Wentzcovitch, QUANTUM ESPRESSO: a modular and open-source software project for quantum simulation of materials, J. Phys.: Condens. Matter 21 (2009) 395502. doi:10.1088/0953-8984/21/39/395502.

[58] P. Giannozzi, O. Andreussi, T. Brumme, O. Bunau, M. B. Nardelli, M. Calandra, R. Car, C. Cavazzoni,

View Article Online
DOI: 10.1039/D6CP01070A

D. Ceresoli, M. Cococcioni, N. Colonna, I. Carnimeo, A. D. Corso, S. de Gironcoli, P. Delugas, R. A. DiStasio, A. Ferretti, A. Floris, G. Fratesi, G. Fugallo, R. Gebauer, U. Gerstmann, F. Giustino, T. Gorni, J. Jia, M. Kawamura, H.-Y. Ko, A. Kokalj, E. Küçkbenli, M. Lazzeri, M. Marsili, N. Marzari, F. Mauri, N. L. Nguyen, H.-V. Nguyen, A. O. de-la Roza, L. Paulatto, S. Poncé, D. Rocca, R. Sabatini, B. Santra, M. Schlipf, A. P. Seitsonen, A. Smogunov, I. Timrov, T. Thonhauser, P. Umari, N. Vast, X. Wu, S. Baroni, Advanced capabilities for materials modelling with quantum ESPRESSO, J. Phys: Cond. Matter 29 (46) (2017) 465901. doi:10.1088/1361-648x/aa8f79.

[59] A. Dal Corso, PSLibrary: A library of ultrasoft and PAW pseudopotentials, https://dalcorso.github.io/pslibrary/ (January 2026).

[60] A. Dal Corso, Pseudopotentials periodic table: From H to Pu, Comput. Mater. Sci. 95 (2014) 337.

[61] J. Bolin, A. Goold, O. Hildeberg, A. Limbäck, E. Schröder, A DFT study of amino acids on Mg and Mg-based alloys (2026). arXiv:2601.07680.

[62] M. Naurin, S. Aldhaim, M. Elliver, L. Hagby, J. D. Nilsson, E. Schröder, Toward an understanding of magnesium in a biological environment: A density functional theory study, AIP Adv. 16 (2026) 065004. doi:10.1063/5.0332131.

[63] H. J. Monkhorst, J. D. Pack, Special points for Brillouin-zone integrations, Phys. Rev. B 13 (1976) 5188. doi:10.1103/PhysRevB.13.5188.

[64] A. Jain, S. P. Ong, G. Hautier, W. Chen, W. D. Richards, S. Dacek, S. Cholia, D. Gunter, D. Skinner, G. Ceder, K. A. Persson, Commentary: The Materials Project: A materials genome approach to accelerating materials innovation, APL Materials 1 (1) (2013) 011002. doi:10.1063/1.4812323.

[65] A. S. Posner, A. Perloff, A. F. Diorio, Refinement of the hydroxyapatite structure, Acta Cryst. 11 (1958) 308–309. doi:10.1107/S0365110X58000815.

[66] J. Åkesson, O. Sundborg, O. Wahlström, E. Schröder, A van der Waals density functional study of chloroform and other trihalomethanes on graphene, J. Chem. Phys. 137 (17) (2012) 174702. doi:10.1063/1.4764356.

View Article Online
DOI: 10.1039/D6CP01070A

DATA AVAILABILITY

Atomic coordinates are available within the supplementary material of the article.